# Modeling and Simulation of a Hydrokinetic Generation Connected to the Electricity Grid

**Julio C. O. de S. Lescano** * **Luigi G. Junior** ** **Hugo C. S. Souza** ***
**Thyago Estrabis** **** **Gabriel Gentil** † **Raymundo Cordero** ‡

* *Federal University of Mato Grosso do Sul, MS, (e-mail: julio.lescano@hotmail.com).*
** *Federal University of Mato Grosso do Sul, MS, (e-mail: luigi.galotto@ufms.br).*
*** *Federal University of Mato Grosso do Sul, MS, (e-mail: hugo.c@ufms.com.br).*
**** *Federal University Rio de Janeiro, RJ (e-mail: thyago.estrabis@gmail.com)*
† *Federal University Rio de Janeiro, RJ (e-mail: gabrielgent@gmail.com)*
‡ *Federal University of Mato Grosso do Sul, MS, (raymundo.garcia@ufms.br).*

**Abstract:** As conventional hydroelectric power plants are reaching physical and environmental constraints, hydrokinetic turbines, which use only a natural flow from the rivers analogous to wind generation, may become a growing solution to overcome these limits. There is still an unexplored hydropower potential, which is more ecologically correct to take advantage of in a distributed and not dammed way. This paper describes a power converter topology and a control system for a hydraulic turbine to inject power into the grid proportional to the river flow rate. The control system is composed of: an MPPT (Maximum Power Point Tracking), which measures the voltage and current in the DC bus and generates a voltage reference of the DC link for the maximum power of the turbine-generator system; by the DC link voltage controller, which provides a reference for the control of electric current injection into the network; and by the single-phase instantaneous current control of the grid-connected voltage source inverter. One of the contributions consists of identifying the operating conditions and limits of the whole system, composed of the hydraulic turbine, the electric generator, and the power converter. The same methodology may be applied to design specific sets of a turbine-generator-converter system for each application.

*Keywords:* Hydrokinetic; MPPT; Grid-Connected; Control System.

## 1. INTRODUCTION

The growing investments in renewable energy matrices are observed in the World due to environmental issues and electricity demand. In Brazil, hydroelectric generation stands out, with more than 60% of the electricity matrix, and the distributed generations are mainly photovoltaic, as shown in Assad and Batista (2018). The predominant hydroelectric power plants have relevant environmental impacts, as it needs water dam and large area reservoirs. This is an important requirement to consider while choosing the place for new installations, which are deeply dependent on geographic characteristics. Therefore, they are unfeasible for distributed generations, even with hydraulic resources available. For these applications, the harnessing of the kinetic energy of the rivers (without damming) in a distributed way presents good expectations of feasibility (Troullaki et al. (2019); Rana and Meena (2018)).

The hydrokinetic generators do not need the accumulation of water mass since they are dimensioned for river flow (Buswig et al. (2020)). As it does not have a reservoir, it does not have flow control, causing the energy produced to depend directly on the river's flow. In times of drought, there is a reduction in the energy capacity produced, and they should be used complementary to the electric grid or to a microgrid (Rajagopal and Singh (2011); Rathore and Singh (2014); Chen et al. (2019)).

In Albarello (2014), a run-of-river SHP is presented when the river's drought flows are equal to or greater than the flow required so that the generated power is greater than the expected demand for the application. The adduction system shall be designed to conduct the discharge necessary to supply the power that meets the maximum demand. The local energy use will be partial, and the spillway will always work, overflowing with excess water. This category of SHP presents, among others, the following simplifications: it does not require flow regularization

studies, it does not require load seasonality studies, and it facilitates the studies and design of the water intake.

Yuen et al. (2013) has developed a control system for a hydrokinetic energy converter, which will be used in an experimental station in Sweden. The project uses a vertical axis hydrokinetic turbine connected to a permanent magnet generator, a control system, and a ground station for energy delivery.

Kerdtuad et al. (2018) establish the generation of a micro hydropower plant using permanent magnet synchronous generator (PMSG) and supply power to a micro grid. A Pelton turbine coupled to the generator was used, connected to a step-up transformer. A conventional two-stage converter topology receives the variable voltage at the transformer output for controlled connection to the electrical grid.

This work developed a model of a hydrokinetic generation system, which may be used to analyze and design the set of turbine-generator-converter, and the proper control for each application. The converter topology limits are analyzed with the model in off-grid exhaustive simulations.

## 2. PRESENTED SYSTEM OVERVIEW

Fig. 1 shows the schematic overview of the system with the main control blocks for grid-connected operation. The turbine was modeled based on real data of an experimental setup. The system is operating with PMSG and a usual two-stage converter.
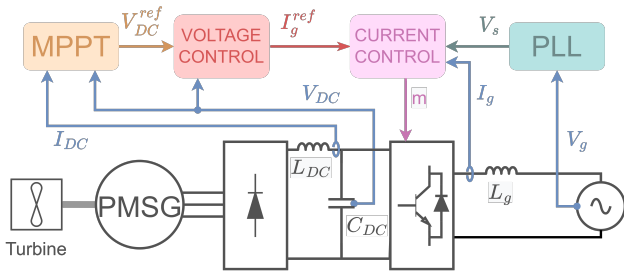


Figure 1. Schematic Diagram of the Presented System.

The three-phase PMSG was chosen for its simplicity and high power density, considering the operating voltage range. A three-phase rectifier is connected to the generator's output and has an LC low pass filter in the output to regulate the DC-link.

The DC link voltage $V_{DC}$ and current $I_{DC}$ signals are used for the MPPT (Maximum Power Point Tracking) that uses the P&O (perturb and observe) strategy. The output of the MPPT will be the voltage reference $V_{DC}^{ref}$ for the DC-link voltage control system. Furthermore, the output of the voltage control is the reference $I_g^{ref}$ for the grid current control, which also uses the reference signal $V_s$ given by the PLL (Phase-Locked Loop).

The DC link is the input of a single-phase voltage source inverter (VSI) controlled by the current control system to modulate the grid current through the coupling inductor $L_g$.

All model components were designed accordingly to the following system requirements on Table 1.

Table 1. System Requirements

| Variable | Description | Value |
|----------|-------------|-------|
| $V_g^{RMS}$ | RMS Grid Voltage | $127V$ |
| $f_g$ | Grid frequency | $60Hz$ |
| $P_M^{max}$ | Maximum mechanical power | $1kW$ |
| $v_f^{max}$ | Maximum water speed | $15m/s$ |
| $v_f^{min}$ | Minimum water speed | $10m/s$ |

## 3. TURBINE MODEL

The basic theory of a hydraulic kinetic power converter's operation is similar to a wind farm. The differences are related to a higher density of water, the presence of the water's surface, resource turbulence, and predictability. Then, the turbine model is developed similarly to wind turbines, where the Steady-State Efficiency ($C_p$) is defined in function of the Tip-Speed-Ratio (TSR), in Equation 1.

$$TSR = \lambda = \frac{\omega \times r}{v_f} \qquad (1)$$

Where $\omega$ is the turbine rotation, $r$ is the turbine radius, and $v_f$ is the fluid velocity. The TSR or $\lambda$ is variable accordingly to the mechanical load.

The turbine efficiency ($C_p$) is a relation of the mechanical power ($P_M$), in Equation 2, by the Hydraulic power ($P_H$), in Equation 3.

$$P_M = m_p.g.l.\omega \qquad (2)$$

The variables $m_p$, $g$, and $l$ are mass measured on Prony's balance, gravitational acceleration, and Prony's test bar length, respectively.

The hydraulic kinetic power, in (3), is dependent on the mass water flow ($m_f/t = A_u.\rho.v_w$). Since the useful turbine area, $A_u$, and fluid density $\rho$ area constant, the available hydropower is variable with the cube of the fluid speed.

$$P_H = \frac{m_f.v_f^2}{2.t} = \frac{1}{2}A_u.\rho.v_f^3 \qquad (3)$$

In Equation 4, the previous are combined in order to obtain an algebraic expression of $C_p(\lambda)$.

$$C_p(\lambda) = \frac{P_M}{P_H} = \frac{m_p.g.l.\omega}{\frac{1}{2}A_u.\rho.v_f^3} = \left(\frac{2.g.l}{A_u.\rho}\right)\frac{m_p.\omega}{v_f^3} \qquad (4)$$

An experimental bench with a Pelton turbine (Figure 2), presented in Lescano et al. (2017), was used to get the steady-state dataset with $\omega$, $P_H$, $P_M$ for different operational points with controlled $v_f$ and $m_p$.

The data is then normalized using (1) and (4), and a parametric regression model, in Equation 5, is performed
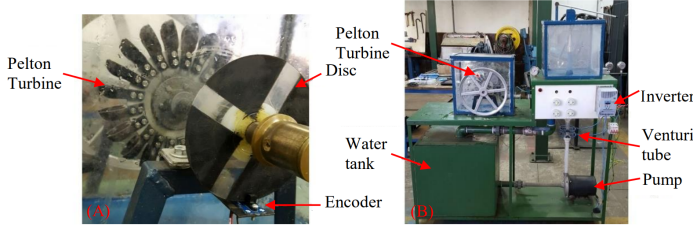
Figure 2. Pelton Turbine Experimental Bench.

to fit the $C_p(\lambda)$ data into a third-order polynomial function (Shokrzadeh et al. (2014)).

$$\widehat{C_p}(\lambda) = \beta_0 + \beta_1\lambda + \beta_2\lambda^2 + \beta_3\lambda^3 \qquad (5)$$

Figure 3 presents the normalized data and the fitted curve. This curve provides an estimation of the turbine efficiency $\widehat{C_p}$ as a function of the TSR.
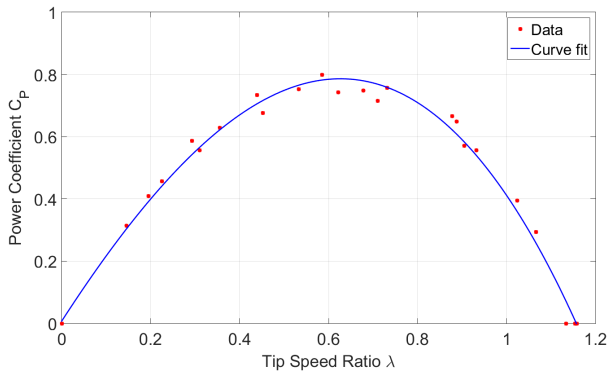


Figure 3. Pelton Turbine $C_p \times \lambda$ data and fit.

The model is defined by (6), with coefficient of determination $R^2 = 0.9849$.

$$\widehat{C_p}(\lambda) = 0,005209 + 1,52\lambda - 0,669\lambda^2 - 0,3915\lambda^3 \quad (6)$$

With the polynomial coefficients, the turbine is implemented in the simulation as shown in Figure 4. This subsystem uses fluid velocity and rotation to calculate $\lambda$. Then, the regression model calculates the estimated efficiency.

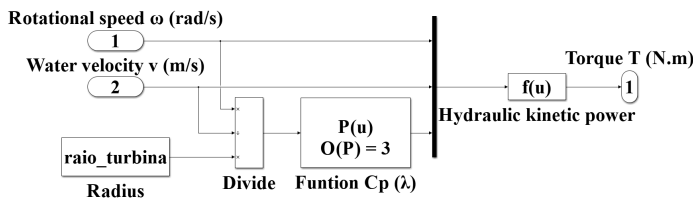

Figure 4. Model of the Pelton Turbine in steady state.

The turbine torque is calculated using Equation 7.

$$T = \widehat{C_p}(\lambda).\frac{P_H}{\omega} = \widehat{C_p}(\lambda).\frac{A_u.\rho.v_f^3}{2.\omega} \qquad (7)$$

## 4. GENERATOR AND CONVERTER MODELS

The generator, the rectifier, and the inverter were implemented using the existent Simscape block sets in Matlab/Simulink.

### 4.1 Generator Sizing

The generator was dimensioned, considering the application's maximum and minimum rotation expected (Table 1). The minimum DC-link voltage needed to modulate the grid voltage is used to determine the generator induction at the minimum speed. Similarly, the maximum voltage designed accordingly to the power semiconductors limits is related to the maximum speed. So the model does not need a boost stage such as a transformer or DC-DC converter.

The PMSG block was used setting the DC generator voltage constant $K_{DC}$, in (8), where $n_m min$ is the minimum machine rotation (in RPM).

$$K_{DC} = 1000\frac{V_g^{RMS}\sqrt{2}}{n_m^{min}} \qquad (8)$$

To dimension the minimum machine rotation, the $v_f^{min}$ requirement (Table 1) is combined with $\lambda = 0.6272$ (for maximum $C_p$ based on (6)) to calculate the rotation with (1). The value of this rotation is approximately 60 rad/s (573 rpm), resulting in $K_{DC} = 313.47$.

### 4.2 Converter Sizing

The rectifier is an ideal, average full-wave model, and the inverter is the ideal VSI average model. The $L_{DC}$ and $C_{DC}$ components were calculated considering the double of the grid frequency as bandwidth. Capacitance is also needed for power decoupling between the grid and the generator.

The converter parameters are presented in Table 2.

Table 2. Converter parameters

| Variable | Description | Value |
|---|---|---|
| $V_{DC}^{min}$ | Minimum DC link Voltage | $200V$ |
| $V_{DC}^{max}$ | Maximum DC link Voltage | $400V$ |
| $f_s$ | Switching frequency | $30kHz$ |
| $C_{DC}$ | DC link Capacitance | $820\mu F$ |
| $L_{DC}$ | DC link Inductance | $2.1mH$ |
| $\Delta i_{Lg}$ | inductor current ripple | $35\% \times 8A$ |
| $L_g$ | Grid inductance | $3mH$ |
| $R_g$ | Grid resistance | $0.1\Omega$ |

The grid coupling inductor was calculated using the Equation (9) for the worst-case condition on the maximum DC link voltage. The resistance is related to the chosen conductor, as typical of a constructed inductor.

$$L_g = \frac{\left(V_{DC}^{max} - V_g^{RMS}\sqrt{2}\right).m}{\Delta i_{Lg}.f_s} \qquad (9)$$

The DC link voltage range chosen was 200 Volts for the lower limit (enough to modulate $V_g^{RMS}$) and 400 Volts for the upper limit, related to the physical limits of the converter components.

## 5. CONTROL SYSTEM DESIGN

The project control system starts from the MPPT, which continuously searches for the point of maximum operating power. The MPPT generates a reference voltage for the voltage controller, which generates a current reference for the current controller. The current controller generates a modulating signal for the VSI for grid connection.

### 5.1 MPPT: Maximum Power-Point Tracking

The MPPT algorithms (de Brito et al. (2011); Brandão and Marafão (2016)) are widely applied in renewable generation, mainly for wind or photovoltaic systems (Bollipo et al. (2020); Abo-Khalil and Dong-Choon Lee (2008)), but also for hydraulic generation (Belhadji et al. (2013); Molina and Pacas (2010)). This work was applied in the model the P&O MPPT with variable step.

The MPP of this hydraulic system varies with the river's flow, rotation, and torque obtained in the turbine. So, MPPT algorithms are challenged to track the MPP providing the DC link control loop reference quickly. The system will use the MPP of the turbine, generator, and rectifier set since it is desired to install electrical (Voltage and Current) sensors instead of mechanical (Torque and Speed) sensors. Therefore, the MPPT is implicitly considering the generator and the rectifier efficiency.

To better explain the MPPT operation, it is presented in Figure 5a the Current × Voltage ($I × V$) characteristic curve of the system for a fixed flow. The short circuit point $(0, I_{sc})$ and the open circuit point $(V_{oc}, 0)$ are also indicated. For the same flow, it is also presented the Power × Voltage ($P × V$) curve, in the Figure 5b, with the MPP represented by $(V_{MPP}, I_{MPP})$.

The variable step MPPT P&O was implemented using an algorithm presented in Galotto Jr (2011), as shown in Figure 6. In the block diagram highlighted in red, the power ($P = V.I$) and the derivatives $\frac{dV}{dt}$ and $\frac{dP}{dt}$ are calculated to determine the step direction. The block diagram highlighted in violet calculates the step size considering the power variation for the output variation. If necessary, the MPPT block has an inverse option configuration, as seen in the green area.
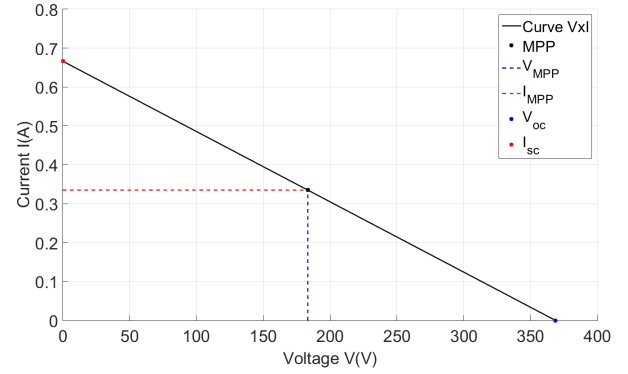
### 5.2 DC link voltage controller

The DC link voltage controller was tuned using the transfer function $G_{vi}$ (10), which represents the dynamic variation of the DC voltage for a grid current disturbance.

$$G_{vi} = \frac{V_g^{RMS}\sqrt{2}}{2V_{DC}C_{DC}.s} = \frac{179.6}{0.3608s} \quad (10)$$
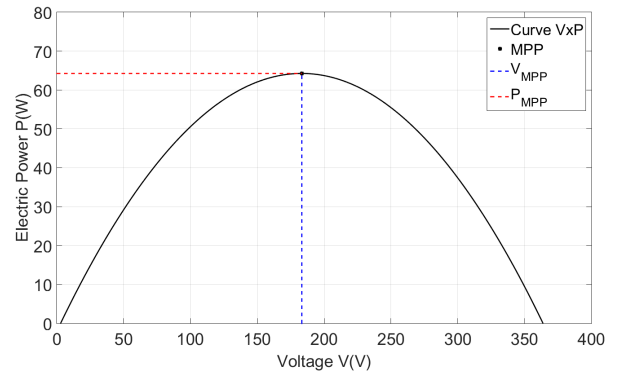
Therefore, the PI of the voltage controller is:

$$PI = 0.1219 + \frac{2.0526}{s} \quad (11)$$

Note that the system has a phase margin of 75° as a dynamic requirement.



(a) Current (A) × Voltage (V)



(b) Power (W) × Voltage (V)

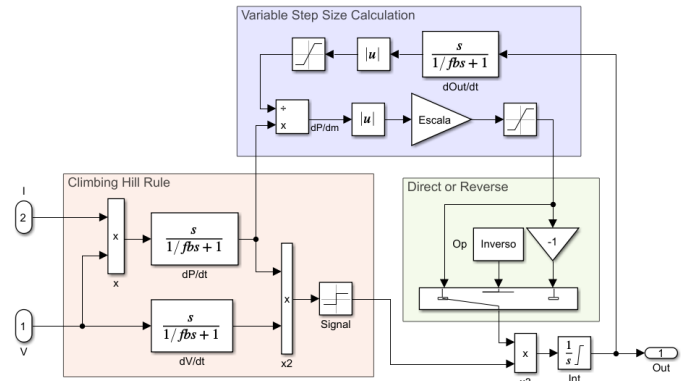Figure 5. Curves of the hydraulic system



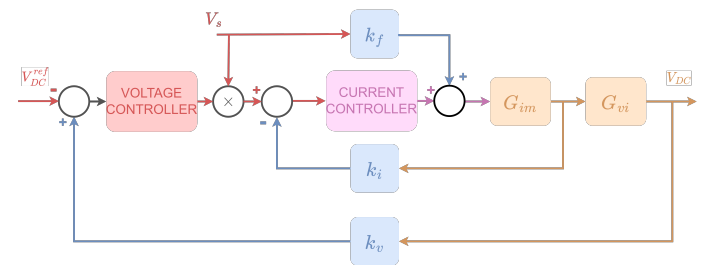Figure 6. Block diagram of the simulated MPPT.



Figure 7. Control System Block Diagram.

The output of the voltage controller is the reference current $I_g^{ref}$ to the current control loop (Figure 7).

The gains $k_i$ and $k_v$ are the sensor gains, which were considered unitary. The $k_f$ is the feedforward gain calculated to reproduce the grid voltage in the VSC output voltage, as shown in (12).

$$k_f = \frac{V_g^{RMS}\sqrt{2}}{V_{DC}^{mean}} \qquad (12)$$

### 5.3 Grid current controller

The current control has the transfer function $G_{im}$ (13), which represents the linearized dynamic variation of the grid current for modulation index variation.

$$G_{im} = \frac{V_{DC}}{(L_g.s + R_g)} = \frac{200}{0.003s + 1} \qquad (13)$$

The plant has a phase margin of 90° and the contribution of $Phase_{PI}$ to 60° is $-30°$.

The current controller PI is in the equation (14).

$$PI = 0.1853 + \frac{1.6885 \times 10^3}{s} \qquad (14)$$

The system phase margin was designed at 60°.

### 5.4 PLL: Phase-Locked Loop

The PLL algorithm is necessary to identify the frequency and phase of the grid. In the block diagram, in Figure 8, PD is a phase detector, which generates a signal proportional to the phase difference between the input and the estimated signal. The LF is the Filter Loop, a low-pass PI that attenuates frequencies above the phase detector and is responsible for the PLL dynamics. Moreover, VCO is the oscillator, which generates the alternating signal based on the loop block output of the system.
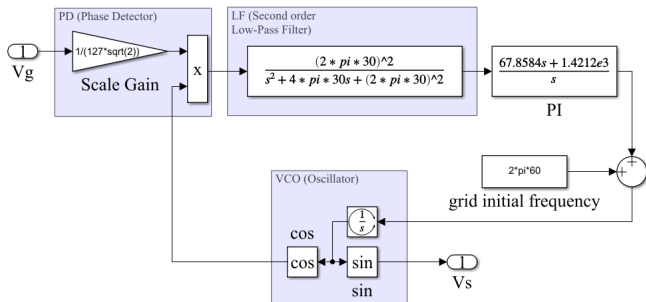


Figure 8. Block diagram of the PLL system.

This PLL will have a gain crossover frequency at 6 Hz, a decade below the grid frequency, and a damping coefficient $\xi = 0.9$. A type 2 system presents a null error at the ramp and step input.

Therefore:

$$\omega_n = 2.\pi.f_c = 37.7 rad/s \qquad (15)$$

$$K_p = 2.\xi.\omega_n = 67.86 \qquad (16)$$

$$K_i = \omega_n^2 = 1421.3 \qquad (17)$$

Thus, the gain $K_p$ and $K_i$ of the compensator PI.

## 6. SIMULATED RESULTS

The system was simulated on Matlab/Simulink, and the complete simulation model is presented in Figure 9.

### 6.1 Transient Results

A simulation with three different flow steps was then performed to observe the system's behavior. The flows chosen were $0.0024\,\text{m}^3/\text{s}$, $0.0018\,\text{m}^3/\text{s}$ and $0.0036\,\text{m}^3/\text{s}$ and are shown in the Figure 10.

In Figure 11, the voltage control system tracks the reference DC link voltage generated by the MPPT. The approximate steady-state voltage observed for the intervals $t = 0 - 2$, $t = 2 - 4$ and $t = 4 - 6$ seconds were 350 V, 260 V and 400 V, respectively. At the flow rate of $0.0036\,\text{m}^3/\text{s}$, the MPPT is saturated at the upper limit due to the DC link voltage limit designed for the converter. In this saturation condition, the system does not operate in MPP but continues to work at the technical voltage limit, prioritizing the integrity of the converter.

Figure 12 shows the transient negative step response of the current injected into the grid under the flow reduction. Even with the change, the system keeps the phase and frequency synchronized, having a steady-state error in the tracking. The type expects this error of controller designed, different from resonant or synchronous reference techniques known in the literature, to eliminate this error. However, this was unnecessary because the reference is variable by the MPPT, which observes if the maximum power condition was reached regardless of the practical value of the network current.

Figure 12 also presents the control system reacting to the change of flow ascending step. It occurs as in the descending step, maintaining phase and frequency, with minor steady-state errors.

In the power graph (Figure 13), one can see the rise and settling time for each input step, the efficiency of each system conversion being implicit. The greatest power loss occurs when converting hydraulic kinetic energy to mechanical energy.

In the figure 14, the variable-pitch MPPT allows a relatively fast MPP tracking transient and practically no oscillations in a steady state, stabilizing around the maximum efficiency. The turbine predominantly determines the system's maximum efficiency, which is 78,61%. This is because the efficiency of the electric generator and the rectifier is higher than the turbine's efficiency. Note that the first and second entry steps are in the controllable region, thus achieving this efficiency. In the third inlet flow, there was saturation of the MPPT, as can also be seen in Figure 11. Note that the efficiency drops to 72,34%, so the DC link voltage does not operate above the maximum voltage designed for the converter.
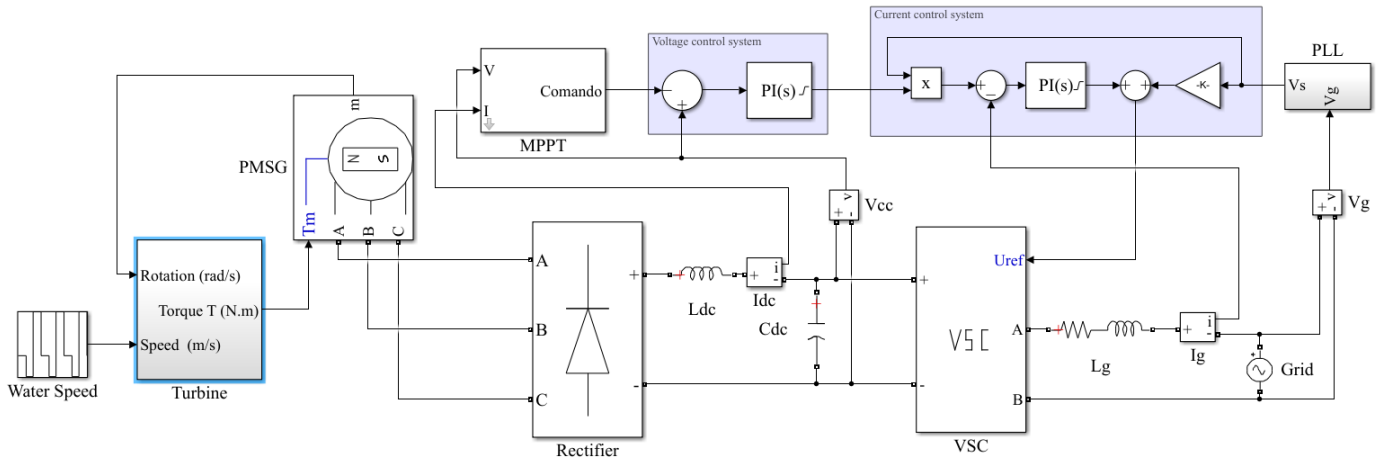
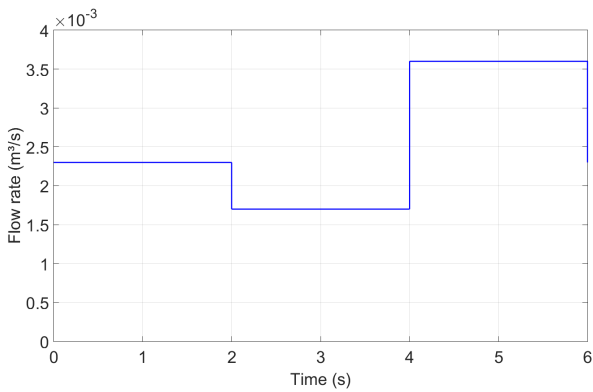Figure 9. System simulated in *Simulink/Matlab*.
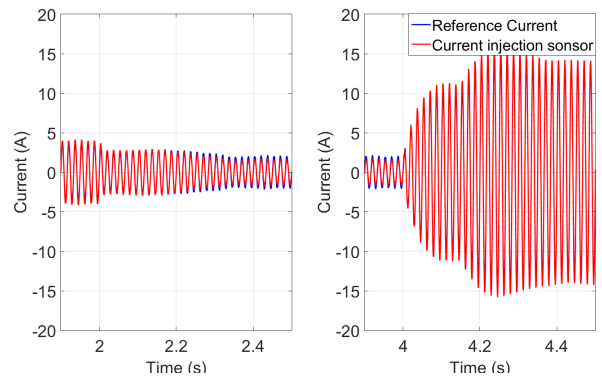


Figure 10. Flow $Q(m^3/s)\times$ Time $(s)$.



Figure 12. Current Control $I(A)\times$ Time $(s)$ for $t = 1, 9$ to $t = 2, 5$ and $t = 3, 9$ to $t = 4, 5$.
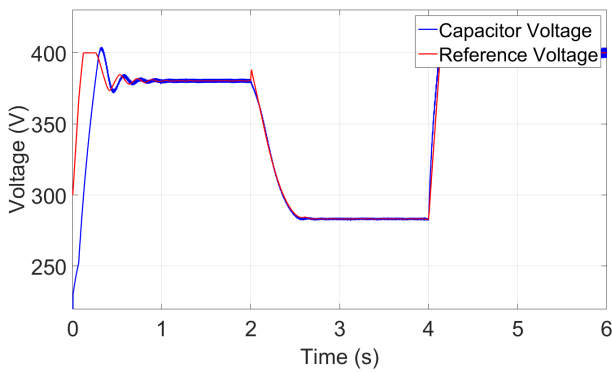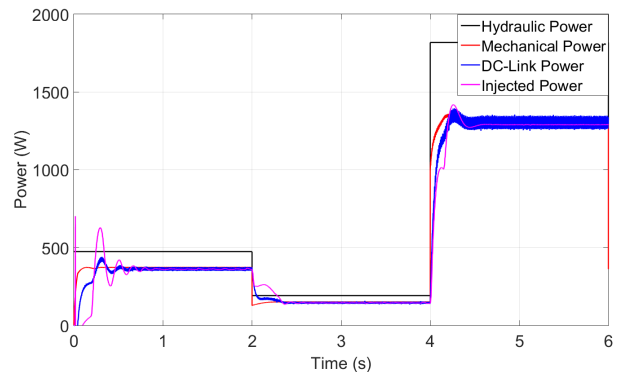


Figure 11. DC link Voltage (V) $\times$ Time (s).

### 6.2 Steady state results: characteristic curves

The system was isolated from the grid to obtain the power characteristic curves, using only the turbine, the permanent magnet generator, and the rectifier, with a resistive load, as seen in Figure 15:

The system was simulated, changing the flow input and the load resistance, with the flow varying from $0.0011\,\mathrm{m^3/s}$ to $0.0035\,\mathrm{m^3/s}$, with a step of $0.0001\,\mathrm{m^3/s}$ and resistance ranging from $10\,\Omega$ to $10.000\,\Omega$. All data were obtained in a steady state.



Figure 13. Power (W) $\times$ Time (s).

In Figure 16, the vertical bars in red represent the operational voltage limits of the DC link for the electronic power converter. Different converters can operate with different limits depending on the topology and semiconductors. The increase in this range is possible for greater energy use and an increase in the cost and complexity of the converter. Thus, it is a challenging engineering design problem that can still add turbine change, electric generator change, and set optimization.
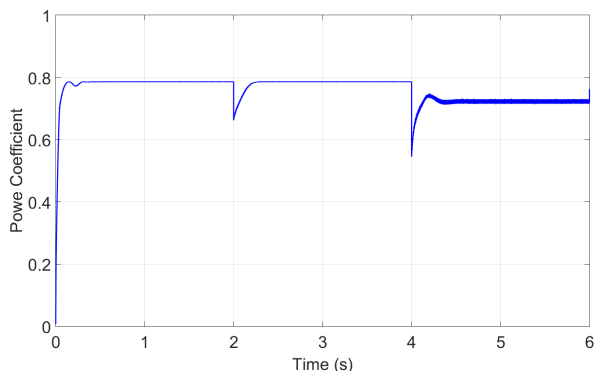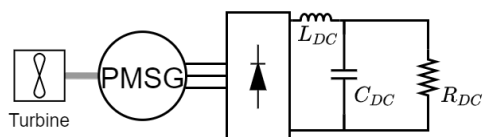
Figure 14. Power Coefficient × Time (s).



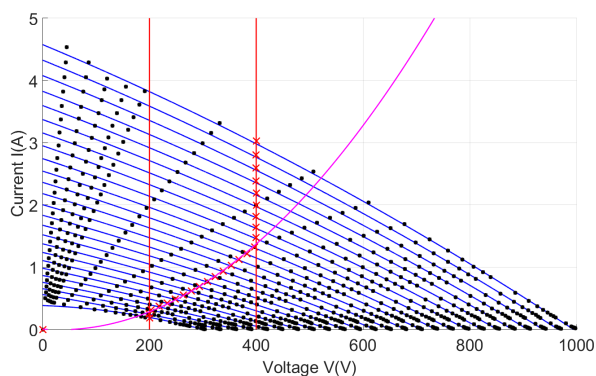Figure 15. System simulation diagram to obtain the characteristic curve.



Figure 16. Graph Curve Current I(A) × Voltage V(V).

The black asterisks represent the steady state of each simulation for each combination of flow and load resistance. The blue curves are the linear regression for each flow input varying only the resistance, that is, the characteristic curve for each inlet flow. The red asterisks are the maximum power achievable with the converter for each input flow. In magenta is the maximum power curve of the system.
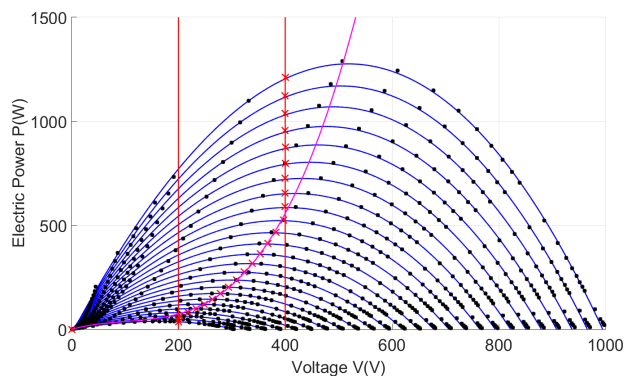


Figure 17. Graph Power Curve $P(W)$ × Voltage $V(V)$.

The Figure 17 has the curve Voltage $V(V)$ × Power $P(W)$, which has the same description as the figure 16. Note that, at the highest flow, the system does not have the maximum power in the controlled area, making it necessary to saturate the upper voltage. For this reason, the efficiency is reduced, and the same occurs for the curve at the lower limit when the maximum power voltage is below the minimum limit necessary for the modulation of the inverter. However, the system injects power, even if not at the best efficiency.

## 7. CONCLUSION

The kinetic energy hydraulic generation can be an efficient alternative with less environmental damage since it does not need dams, having a greater need for studies in the area.

The model developed for the Pelton Turbine has advantages in obtaining it since, after the Prony test, the characteristic curve of the turbine in steady-state is obtained. Being able to expand the scale without the need for new simulations or experiments, as long as the geometric characteristics are maintained, such as, for example, the number of blades, the proportion of the turbine and injector system.

The curve presented in Figure 17 demonstrates an essential contribution of this work, which consists of the analysis of the operation of the hydraulic turbine together with the permanent magnet generator and the rectifier. This way, it was possible to identify the voltage and power of the set available for each value of turbine inlet flow. The maximum power points of this system were also highlighted as a function of the flow and the physical voltage limits chosen for the operation of the inverter to be connected to the electrical grid.

In addition to allowing the exchange of primary machines, the simulation system developed can also be used to dimension different combinations of electrical generators and topologies of electronic power converters. Future works can also be done to evaluate and optimize these combinations.

Although simple, the voltage and current control system present satisfactory results because the MPPT seeks maximum power even if there is a steady-state error in tracking the control loops. The variable-pitch MPPT presents significant advantages for the system, making it faster in the transient and stable in the steady state. The system has a controllable region determined by the minimum and maximum voltage limitations on the DC link of the converter topology. At voltages within these limits, the system operates at maximum efficiency, but outside the controllable area of the system, power injection into the network remains less efficient in maintaining safety voltages.

## REFERENCES

Abo-Khalil, A. and Dong-Choon Lee (2008). MPPT Control of Wind Generation Systems Based on Estimated Wind Speed Using SVR. *IEEE Trans. Ind. Electron.*, 55(3), 1489–1490. doi:10.1109/TIE.2007.907672. URL http://ieeexplore.ieee.org/document/4390608/.

Albarello, L. (2014). Guia para a implantaÇÃo de pequenas centrais hidrelÉtricas - pch's. *Dissertação (Curso de pós-graduação em eficiência energétoca aplicada aos processos produtivos, Universidade Federal de Santa Maria.* URL https://repositorio.ufsm.br/bitstream/handle/1/1366/Albarello_Leonardo.pdf?sequence=1.

Assad, V.C.D. and Batista, O.E. (2018). Scenario and perspective of distributed generation in Brazil. In *2018 Simposio Brasileiro de Sistemas Eletricos (SBSE)*, 1–5. IEEE, Niteroi. doi:10.1109/SBSE.2018.8395706. URL https://ieeexplore.ieee.org/document/8395706/.

Belhadji, L., Bacha, S., Munteanu, I., Rumeau, A., and Roye, D. (2013). Adaptive MPPT Applied to Variable-Speed Microhydropower Plant. *IEEE Trans. Energy Convers.*, 28(1), 34–43. doi:10.1109/TEC.2012.2220776. URL http://ieeexplore.ieee.org/document/6332493/.

Bollipo, R.B., Mikkili, S., and Bonthagorla, P.K. (2020). Hybrid, optimization, intelligent and classical PV MPPT techniques: Review. *CSEE JPES*. doi:10.17775/CSEEJPES.2019.02720. URL https://ieeexplore.ieee.org/stamp/stamp.jsp?tp=&arnumber=9171659.

Brandão, D.I. and Marafão, F.P. (2016). DIGITAL PROCESSING TECHNIQUES APPLIED TO POWER ELECTRONICS. In *Modeling Power Electronics and Interfacing Energy Conversion Systems*, 279–320. John Wiley & Sons, Inc., Hoboken, NJ, USA. doi:10.1002/9781119058458.ch12. URL https://onlinelibrary.wiley.com/doi/10.1002/9781119058458.ch12.

Buswig, Y.Y., Affam, A., bin Othman, A.K.H., bin Julai, N., Sim, Y.S., and Mulyo Utomo, W. (2020). Sizing of a Hybrid Photovoltaic-Hydrokinetic Turbine Renewable Energy System in East Malaysia. In *2020 13th International UNIMAS Engineering Conference (EnCon)*, 1–8. IEEE, Kota Samarahan, Malaysia. doi:10.1109/EnCon51501.2020.9299329. URL https://ieeexplore.ieee.org/document/9299329/.

Chen, L., Wang, Y., Lu, X., Zheng, T., Wang, J., and Mei, S. (2019). Resilient Active Power Sharing in Autonomous Microgrids Using Pinning-Consensus-Based Distributed Control. *IEEE Trans. Smart Grid*, 10(6), 6802–6811. doi:10.1109/TSG.2019.2911344. URL https://ieeexplore.ieee.org/document/8692619/.

de Brito, M.A.G., Sampaio, L.P., Galotto Jr, L., and Canesin, C.A. (2011). Evaluation of MPPT techniques for photovoltaic applications. In *2011 IEEE International Symposium on Industrial Electronics*, 1039–1044. IEEE, Gdansk, Poland. doi:10.1109/ISIE.2011.5984303. URL http://ieeexplore.ieee.org/document/5984303/.

Galotto Jr, L. (2011). *Inversores integrados monofásicos aplicados em sistemas fotovoltaicos com conexão à rede de distribuição de energia elétrica.* Tese de Doutorado, Universidade Estadual Paulista, Faculdade de Engenharia de Ilha Solteira, Ilha Solteira - SP. URL https://repositorio.unesp.br/handle/11449/100317.

Kerdtuad, P., Simma, T., Chaiamarit, K., and Visawaphatradhanadhorn, S. (2018). Establishment of a Pico Hydro Power Plant Using Permanent Magnet Synchronous Generator Supplied for AC Microgrid. In *2018 International Electrical Engineering Congress (iEECON)*, 1–4. IEEE, Krabi, Thailand. doi:10.1109/IEECON.2018.8712214. URL https://ieeexplore.ieee.org/document/8712214/.

Lescano, J.C.O.d.S., Santos, M.W.M.d., Branco, F.P., Laporte, D.J., and Barbosa, F.M. (2017). Modelling, Control And Measurement Of Pelton Hydraulic Turbine: A Laboratory Case Of Study. Curitiba, PR, Brazil. URL http://www.sistema.abcm.org.br/articleFiles/download/11542.

Molina, M.G. and Pacas, M. (2010). Improved power conditioning system of micro-hydro power plant for distributed generation applications. In *2010 IEEE International Conference on Industrial Technology*, 1733–1738. IEEE, Vi a del Mar , Chile. doi:10.1109/ICIT.2010.5472461. URL http://ieeexplore.ieee.org/document/5472461/.

Rajagopal, V. and Singh, B. (2011). Improved electronic load controller for offgrid induction generator in small hydro power generation. In *India International Conference on Power Electronics 2010 (IICPE2010)*, 1–7. IEEE, New Delhi, India. doi:10.1109/IICPE.2011.5728118. URL http://ieeexplore.ieee.org/document/5728118/.

Rana, K. and Meena, D.C. (2018). Self Excited Induction Generator for Isolated Pico Hydro Station in Remote Areas. In *2018 2nd IEEE International Conference on Power Electronics, Intelligent Control and Energy Systems (ICPEICES)*, 821–826. IEEE, Delhi, India. doi:10.1109/ICPEICES.2018.8897329. URL https://ieeexplore.ieee.org/document/8897329/.

Rathore, U.C. and Singh, S. (2014). Power quality control of SEIG based isolated pico hydro power plant feeding non-linear load. In *2014 IEEE 6th India International Conference on Power Electronics (IICPE)*, 1–5. IEEE, Kurukshetra, India. doi:10.1109/IICPE.2014.7115777. URL http://ieeexplore.ieee.org/document/7115777/.

Shokrzadeh, S., Jafari Jozani, M., and Bibeau, E. (2014). Wind Turbine Power Curve Modeling Using Advanced Parametric and Nonparametric Methods. *IEEE Trans. Sustain. Energy*, 5(4), 1262–1269. doi:10.1109/TSTE.2014.2345059. URL http://ieeexplore.ieee.org/document/6894235/.

Troullaki, A., Latoufis, K., Marques, P., Freire, F., and Hatziargyriou, N. (2019). Life Cycle Assessment of Locally Manufactured Small Wind Turbines and Pico-Hydro Plants. In *2019 International Conference on Smart Energy Systems and Technologies (SEST)*, 1–6. IEEE, Porto, Portugal. doi:10.1109/SEST.2019.8849074. URL https://ieeexplore.ieee.org/document/8849074/.

Yuen, K., Apelfrojd, S., and Leijon, M. (2013). Implementation of Control System for Hydrokinetic Energy Converter. *Journal of Control Science and Engineering*, 2013, 1–10. doi:10.1155/2013/342949. URL http://www.hindawi.com/journals/jcse/2013/342949/.